Optical Vernier Effect Enabled Narrow Linewidth All-Fiber SBS-FWM-Based Tunable Optical Frequency Comb Generation

Aritra Paul, *Student Member, IEEE*, Arunabh Deka, Tanooja Mishra, and Pradeep Kumar Krishnamurthy

***Abstract*—In this paper, we experimentally demonstrate a low-power, broadband, and narrow linewidth SBS-FWM OFC with tunable line spacing of 50 to 600 GHz. The SBS-FWM OFC spans a bandwidth of ≈100 nm over the C+L-band region using ≈15 dBm pump power. The OFC is obtained by cascaded FWM process in highly nonlinear fiber (HNLF), seeded by SBS pumps in an all-fiber ring cavity setup. The linewidth of the SBS-FWM comb lines is measured to be ≈20 MHz which is largely determined by the SBS pump properties. By using the optical Vernier effect, the linewidth of comb lines is reduced by a factor of more than 2000 to below 20 kHz. We utilize the SBS-FWM OFC to study the performance of binary and 4-PAM transmission at 1 and 10 Gbps in a back-to-back (B2B) setup. The side-modes caused by the FP-cavity, formed by the HNLF modules in the ring cavity in our setup, affects the performance of the B2B transmission of PAM system.**

***Index Terms*—Optical frequency comb (OFC), stimulated brillouin scattering (SBS), four-wave mixing (FWM), optical vernier effect (OVE).**

I. Introduction

THE cascaded stimulated Brillouin scattering (SBS) and four-wave mixing (FWM) in all-fiber configuration, have been used in the generation of broadband tunable optical frequency comb (OFC) in the C-band region [1], [2], [3], [4], [5], [6], [7], [8], [9], [10], [11], [12], [13]. The narrow linewidth, low-threshold, phase coherent behaviour of SBS process in silica SMF can generate dense OFCs with fixed line-spacing of ≈11 GHz having >20 MHz linewidth [14], [15], [16], [17]. However, SBS-based comb suffers from low gain and requires Erbium-doped fiber amplifiers (EDFA) and/or pump recycling in a ring configuration to generate a broadband comb [9], [10], [11], [12], [18], [19]. Such techniques limit tunability range due to EDFA self-lasing and restrict the number of comb lines at low operating power [9], [10], [11], [12], [13], [19], [20]. Although the limitations of fixed line-spacing can be eliminated by utilizing multi-Brillouin-spacing based dual ring configuration, it suffers from a limited number of comb lines [16], [21], [22], [23], [24]. Thus, the SBS process is often implemented in conjunction with non-degenerate FWM to achieve a broadband OFC source with excellent tunability in line spacing.

In SBS-assisted FWM-based OFCs, SBS signals act as pumps for cascaded FWM process inside a nonlinear ring cavity [7], [25], [26], [27], [28], [29], [30]. Since FWM is a phase-matched process, the generated comb lines maintain a high degree of coherence among themselves [14]. However, generating SBS pumps in SBS-FWM cavities at a low input power of <15 dBm, require long-length SMF which leads to a cavity FSR typically in the range kHz to few MHz. This allows a large number of longitudinal modes to oscillate under the Brillouin gain curve, and results in the generation of SBS pumps with >20 MHz linewidth [28], [30]. When such SBS pumps are used in cascaded FWM-based OFC generation, the linewidth of the generated comb-lines has the same characteristics linewidth as that of the SBS pump. However, the linewidth associated with the SBS-FWM OFC can be reduced by implementing the optical Vernier effect in composite cavity structures [31]. The optical Vernier effect (OVE) is responsible for selecting the longitudinal modes common to the composite ring cavities which effectively increases the cavity FSR [32]. This allows only a restricted number of modes under the SBS gain curve and limits the linewidth of comb lines in the SBS-FWM OFC. However, the number of generated comb lines is limited and requires >20 dBm input power to generate 100 nm broad comb as given in [31], [33].

In this paper, we experimentally demonstrate a low-powered, broadband, narrow-linewidth SBS-FWM OFC with tunable line spacing using ≈15 dBm pump power. The OFC operates in the C+L-band wavelength regions and has a bandwidth of ≈100 nm (1520 nm to 1610 nm). The OFC line spacing can be tuned from 50 to 600 GHz. The tunability in line spacing was achieved by utilizing two tunable laser sources (TLSs). The TLSs are responsible for generating the wavelength-tunable SBS signals from a 10 km SMF placed inside a unidirectional ring cavity. The SBS signals act as pumps for the cascaded FWM-based OFC generation by utilizing a 200 m HNLF placed inside the

Manuscript received 1 May 2023; revised 22 August 2023; accepted 27 August 2023. Date of publication 30 August 2023; date of current version 11 September 2023. This work was supported by Interdisciplinary Cyber Physical System (ICPS), Department of Science and Technology (DST), India, through Quantum Enabled Science and Technology (QuEST), Theme —1Program (DST\ ICPS\ Theme 1\2019). *(Corresponding author: Aritra Paul.)*

Aritra Paul is with the Photonics Science and Engineering, Indian Institute of Technology Kanpur, Kanpur 208016, India (e-mail: aritrap@iitk.ac.in; aritra4551paul@gmail.com).

Arunabh Deka and Tanooja Mishra are with the Electrical Engineering, Indian Institute of Technology Kanpur, Kanpur 208016, India (e-mail: arunabh@iitk.ac.in; tanoojamis20@iitk.ac.in).

Pradeep Kumar Krishnamurthy is with the Electrical Engineering, Indian Institute of Technology Kanpur, Kanpur 208016, India and also associated with the Photonics Science and Engineering as well as Electrical Engineering of Indian Institute of Technology Kanpur, Kanpur 208016, India (e-mail: pradeepk@iitk.ac.in).

Digital Object Identifier 10.1109/JPHOT.2023.3309954

ring cavity. The narrow linewidth behaviour is achieved by implementing the OVE using Mach-Zehnder interferometric (MZI) setup inside the cavity. The Vernier effect reduces the effective cavity length and increases the cavity FSR above 50 MHz allowing a limited number of longitudinal modes under the gain curve of the SBS pumps. Under the cascaded FWM process, the overall linewidth of the comb lines is reduced. We demonstrate linewidth reduction up to 2000 times compared to SBS-FWM OFC without OVE. The comb lines at the cavity output are isolated and utilized for back-to-back (B2B) pulse amplitude modulation (binary and 4-PAM) at 1 Gbps and 10 Gbps data rates. To the best of our knowledge, this is the lowest pump-power, tunable, narrow linewidth SBS-FWM OFC having ≈100 nm bandwidth from an all-fiber cavity in the 1550 nm wavelength region.

The rest of the paper is organized as follows. In Section II, we present the theoretical background of our experimental setup. In Section III, we describe the experimental setup for narrow linewidth, broadband SBS-FWM OFC generation. In Section IV, we discuss the results of the comb generation process, followed by linewidth reduction utilizing OVE, and also present the results showing the effect of OVE in B2B PAM of isolated OFC lines. Finally, we conclude by summarizing our observations in Section V.

II. Theory

SBS is a nonlinear interaction between pump and back-scattered Stokes waves in presence of an acoustic field. SBS in silica SMFs generates Stokes signal down-shifted in frequency. The frequency downshift is defined by the medium properties [14]. The linewidth of the SBS signal in silica SMF exhibits a Lorentzian profile with FWHM of ≈50 MHz [34], [35].

When the SBS signal is utilized as pump source for FWM-based OFC generation in silica SMF, newly generated frequency components under phase-matched conditions will inherit the properties of the pumps [14], [30], [34]. Hence, the linewidth of comb lines generated in FWM-OFC using SBS signals as the pump sources will exhibit a Lorentzian profile. The optical Vernier effect can be utilized to reduce the overall linewidth of the comb lines generated using the SBS-FWM process.

In the optical Vernier effect (OVE), two or more cavities having slightly different lengths and hence different free spectral ranges (FSRs), are combined into one composite cavity. As a result, only those modes that are common to the composite cavity are transmitted, while the modes that are not common to the composite cavity are suppressed. The amount of suppression depends on the composite cavity structure defining the resulting transmittance function [32]. The FSR $\Delta\nu$ of a ring cavity of length L is given by:

$$\Delta\nu = \frac{c}{nL}, \tag{1}$$

where n is the refractive index and c is the speed of light in vaccum. As shown in Fig. 1(a) and (b), if two cavities of lengths L_1 and L_2, having FSRs $\Delta\nu_1$ and $\Delta\nu_2$ are combined into a single composite ring cavity, the FSR of the coupled cavity is determined by the length difference $\Delta L = L_1 - L_2$. We now

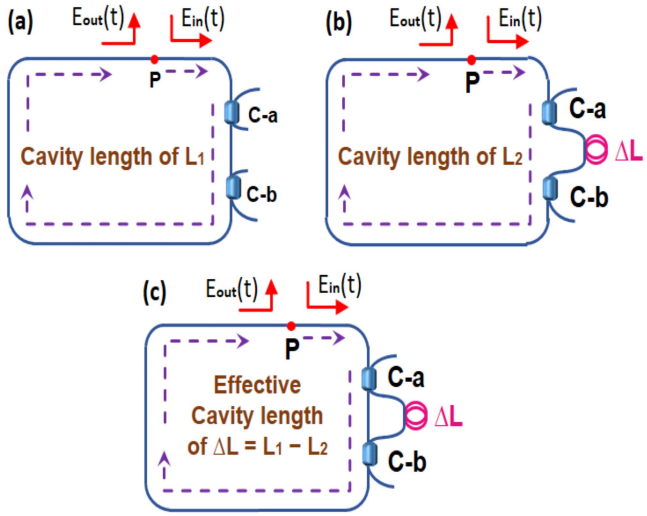

Fig. 1. Schematic representation of the optical Vernier effect.

derive the transmittance of the cavity shown in Fig. 1(c). The OVE cavity, shown in Fig. 1(c), is formed by two 50:50 coupled C-a and C-b, and optical fiber of length L_1 and L_2 with $L_2 = L_1 + \Delta L$ in Mach-Zehnder interferometer (MZI) configuration. Let $E_{in}(t)$ be the electric field launched inside the cavity from a reference point 'P' given as:

$$E_{in}(t) = E_0 e^{j\omega t}, \tag{2}$$

where ω is the optical frequency and E_0 defines the amplitude of the input field. The 50:50 coupler (C-a) divides the input electric field into two equal components $E_1(t)$ and $E_2(t)$ which can then be visualized to propagate separately in the ring cavity having lengths L_1 and L_2 respectively as shown in Fig. 1(a) and (b). The electric field $E_{out}(t)$ at the output of the OVE at point 'P' is given by:

$$E_{out}(t) = \frac{E_0}{2} e^{j\omega\left(t-\frac{nL_1}{c}\right)} + \frac{E_0}{2} e^{j\omega\left(t-\frac{nL_2}{c}\right)}, \tag{3}$$

which can be simplified to obtain:

$$E_{out}(t) = E_0 \cos\left\{\omega n\left(\frac{\Delta L}{2c}\right)\right\} e^{j\omega\left(t-n\left(\frac{L_1+L_2}{2c}\right)\right)} \tag{4}$$

The transmittance of the OVE cavity $T(\omega)$ which is defined as the ratio of time-averaged $E_{out}(t)^2$ and $E_{in}(t)^2$ is given by:

$$T(\omega) = \left(\frac{< E_{out}(t) >}{< E_{in}(t) >}\right)^2 = \frac{1}{2}\left[\cos\left\{\omega n\left(\frac{\Delta L}{2c}\right)\right\}\right]^2 \tag{5}$$

$$= \frac{1}{2}\left[1 + \cos\left\{\omega n\left(\frac{\Delta L}{c}\right)\right\}\right] \tag{6}$$

If we define $\Delta\nu_{OVE}$,

$$\Delta\nu_{OVE} = \frac{c}{n\Delta L} \tag{7}$$

we observe that the transmittance is maximum for those frequencies ω_m for which $\omega_m = K_m \pi \Delta\nu_{OVE}$, where K_m is an even integer and minimum for frequencies $\omega_n = K_n \pi \Delta\nu_{OVE}$ where K_n is an odd integer. From (5) we can observe that the transfer

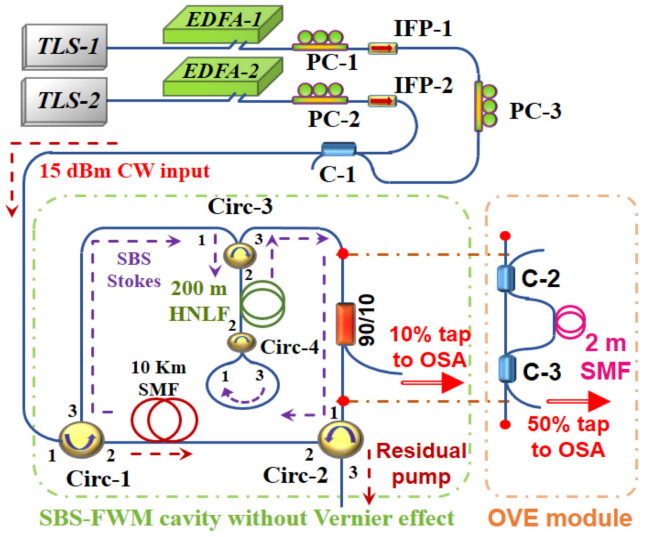

Fig. 2. Experimental setup for SBS-assisted FWM OFC generation and linewidth reduction utilizing optical Vernier effect. TLS: tunable laser source, EDFA: Erbium-doped fiber amplifier, PC: polarization controller, IFP: in-line fiber polarizer, C: 2 × 2 50:50-coupler, Circ: circulator, 90/10: 1 × 2 10% coupler, SMF: single mode fiber, HNLF: highly nonlinear fiber.

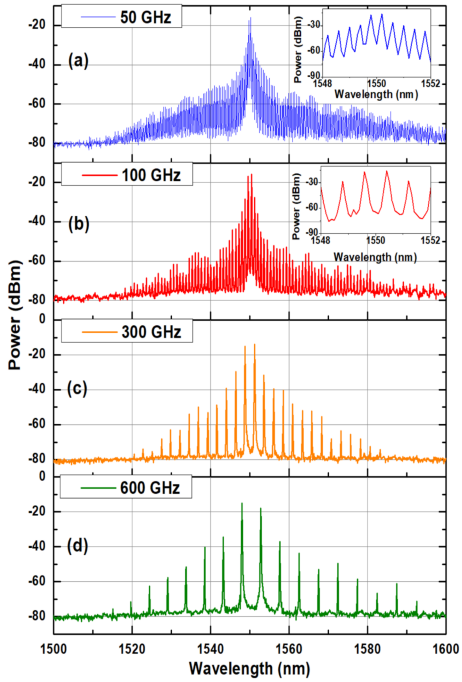

Fig. 3. Measured optical spectra of the OFC generated from SBS-assisted FWM cavity for pump wavelength separation of (a) 50, (b) 100, (c) 300, and (d) 600 GHz. The insets in (a) and (b) show an expanded view of comb lines within a 4 nm span around 1550 nm wavelength for 50 GHz and 100 GHz line-spaced OFC, respectively.

function of the OVE cavity behaves like a filter with sinusoidal edges. Thus, the longitudinal modes that fall within this edge of the filter will also be allowed but their power will decrease as we move away from the peak of the transmittance.

III. Experimental Details

The experimental setup to generate OFC through SBS-assisted cascaded FWM process is shown in Fig. 2. A dual output TLS from Keysight (N77141) supplies two optical waves BP-1 and 2 which act as Brillouin pump sources. The Brillouin pumps (BPs) are amplified to 16 dBm optical power each by two Erbium-doped fiber amplifiers EDFA-1 and EDFA-2 (Optiwave AMP-901 A). After aligning the state of polarization (SOP) of the individual BPs through polarization controllers (PC-1, 2 and 3) and inline fiber polarizers (IFP-1 and 2), they are combined by a 2 × 2 50:50 coupler C-1 and launched into the SBS-FWM cavity as shown in Fig. 2. The use of IFP-1 and IFP-2 also helps in reducing the ASE noise from EDFAs.

The BPs propagating in the 10 km SMF (attenuation (α) = 0.17 dB/km, dispersion coefficient (D) ≈ 18 ps/nm/km, and dispersion slope parameter (S) ≈ 0.1 ps/nm^2/km) in the SBS-FWM cavity generate SBS signals BS-1 and BS-2 which propagate opposite to the direction of pump waves and are coupled to 200 m HNLF (from OFS) through port-3 of the circulator Circ-3. The HNLF used in our experiment has α = 0.5 dB/km, D = ±1 ps/nm/km, S ≈ 0.0064 ps/nm^2/km and is arranged in the dual-pass configuration. The output of the HNLF is coupled back into the cavity through port-1 of circulator Circ-2 thus forming a ring cavity. The HNLF generates FWM OFC through the nonlinear interaction of SBS signals BS-1 and BS-2 via a cascaded FWM process. The SBS-assisted FWM OFC is measured using an optical spectrum analyzer (OSA, Keysight 86412B) at the output of a 1 × 2 10% tap coupler as shown in Fig. 2. We note that the BP frequency separation is set to 50, 100, 300, and 600 GHz to demonstrate the tunability of our OFC line spacing as described in Section IV-A.

We employ OVE to reduce the linewidth of the comb lines of the generated OFC. The OVE cavity is implemented by replacing the 10% tap coupler with a fiber-based MZI using two 2 × 2 50:50 coupler (shown as OVE module in Fig. 2), between ports 3 and 1 of Circ-3 and Circ-2 respectively. The MZI length mismatch (ΔL) of 2 m is obtained by adding a patch cord to one of the arms of the MZI. This results in a composite cavity with FSR of ≈50 MHz. The output of the composite cavity is taken from the open port of the C-3 coupler. The optical spectra of the SBS-FWM OFC with and without OVE are measured using the OSA. The setup for the linewidth measurement of the comb lines and PAM transmission is described in Sections IV-B and IV-C respectively.

IV. Results and Discussions

A. Optical Frequency Comb Spectra

Fig. 3(a) to (d) shows the measured optical spectra of the OFC, generated from the SBS-assisted FWM comb cavity setup shown in Fig. 2 without the optical Vernier effect. The TLS output power is set at −5.5 dBm. The wavelength separation between the two pumps from TLS is varied from 50 to 600 GHz with a central wavelength of 1550 nm. We have kept the minimum wavelength separation between the pumps above 50 GHz in order to maintain the clarity of the measured spectra. This limitation is due to the limited RBW of our OSA and not the setup.

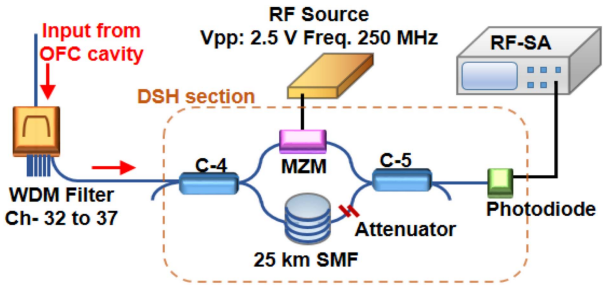

Fig. 4. Delayed self heterodyne (DSH) setup for linewidth measurement of isolated comb lines of the SBS-FWM OFC setup of Fig. 2. WDM: wavelength division multiplexer, C: 2 × 2 50:50-coupler, MZM: Mach-Zehnder modulator, RF-SA: radio frequency spectrum analyzer, SMF: single mode fiber, RF Source: radio frequency source.

The average output power from the SBS-FWM cavity is −6 dBm. As we can see from Fig. 3, a broadband OFC spanning 1520–1610 nm wavelength range is observed at the output of the 10% tap coupler. We also observe that the number of comb lines and power per line decreases as the pump wavelength separation increases. This is due to the increasing phase-mismatch among the generated FWM components as they move away from the zero dispersion wavelength (ZDW) of HNLF and experience higher dispersion as a result. We also observe the effects of modulation instability in the OFC output spectrum as seen in Fig. 3(a) and (b). We attribute this to the net anomalous behaviour of the cavity in the presence of the 10 km SMF. More than 100 lines are observed within a power variation of −60 dB for 100 GHz line separation. The OSNR of the output OFC spectra is >30 dB within a power variation of 40 dB from the spectral peak.

B. Linewidth Measurement Results

In this section, we discuss the optical Vernier effect on the OFC by measuring the linewidth of the individual comb lines. We fix the pump wavelength separation to 100 GHz and isolate the lines using a 16-channel WDM demux. A delayed self-heterodyne (DSH) setup is implemented for the linewidth measurement as shown in Fig. 4. The linewidth of 5 comb lines is measured around the central peak region (1550 nm) of the OFC spectrum including the BS-1 and BS-2 SBS pumps as shown in Fig. 3.

In the DSH setup, the comb line is first divided into two parts using a 50:50 coupler (C-4). The outputs from C-4 are coupled to another 50:50 coupler (C-5) to form an MZI. One arm of the MZI consists of a Mach-Zehnder modulator (MZM, Covega Mach-10) which is used to modulate the comb line with a 250 MHz sinusoidal RF signal from a function generator. The other arm of the MZI consists of a 25 km SMF which acts as the delay line. The DSH output from C-5 is incident on a PIN photodiode (Optilab, PR-10-H-M) for optical-to-electrical conversion and the spectrum of the photocurrent is measured using an RF spectrum analyzer (RF-SA, Keysight N9320B). The RBW and VBW of the RF-SA are set to 10 kHz and 3 kHz respectively. The measured RF spectrum is fit to a Lorentz function. In the following, we only show the results of linewidth measurement for channels 32 to 35. Channel no. 33, 34 correspond to BS-1 and BS-2 respectively, and channel no. 32, 35 correspond comb lines generated due to the cascaded FWM process.

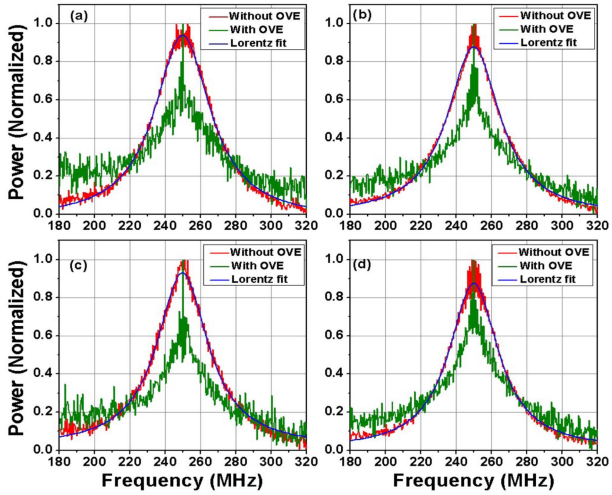

Fig. 5. Comparison of linewidth measurement spectra of comb line corresponding to WDM channels (a) 32, (b) 33, (c) 34, and (d) 35 (140 MHz span) with and without OVE.

As shown in Fig. 5(b) and (c), the SBS pumps generated from the 10 km SMF (Ch. no. 33 and 34), have a measured FWHM linewidth of ≈17 MHz, which is defined by the properties of the SBS process in Silica SMF. Since the acoustic field drives the SBS generation process, we observe that the linewidth of the SBS pumps and the FWM-generated comb line exhibit the same Lorentzian profile (blue curve) [14]. However, for FWM-generated comb lines away from the central wavelength, the linewidth increases. The comb lines at channel numbers 32 (1551.72 nm), 35 (1549.32 nm), and 36 (1548.52 nm) have FWHM linewidth of 19.3, 18, and 20 MHz respectively. The fluctuation at the peak of linewidth spectra corresponds to longitudinal modes with FSR of ≈1 MHz, arising due to the linear Fabry-Pérot (FP) cavity formed by the optical connectors of the two series connected 100 m HNLF modules between Circ-3 and Circ-4.

The 1 × 2 10% tap coupler is replaced with the optical Vernier module having 2 m SMF forming a composite cavity as shown in Fig. 2. The presence of 2 m SMF in one of its arms resulted in an FSR of ≈51 MHz in the OVE ring cavity. The FSR of the OVE ring cavity is more than the FWHM bandwidth of ≈20 MHz of the SBS pumps. To observe the linewidth of the OFC in presence of the optical Vernier effect, the comb lines at the open 50% port of C-3 are isolated using the WDM and observed in the RF-SA using the same DSH method. The results of the linewidth measurement spectra are shown in Fig. 5 (green curves) for WDM channels corresponding to 32 to 35.

From Fig. 5, we observe that there is an overall reduction in the linewidth of the individual comb lines in presence of the optical Vernier effect. Since 50% of the cavity power is extracted out from the cavity (under the Vernier effect), there is an increase in the power of the observed linewidth spectra in the RF-SA. However, we present the data as normalized plots for comparing the linewidth of isolated comb lines, with and without the OVE

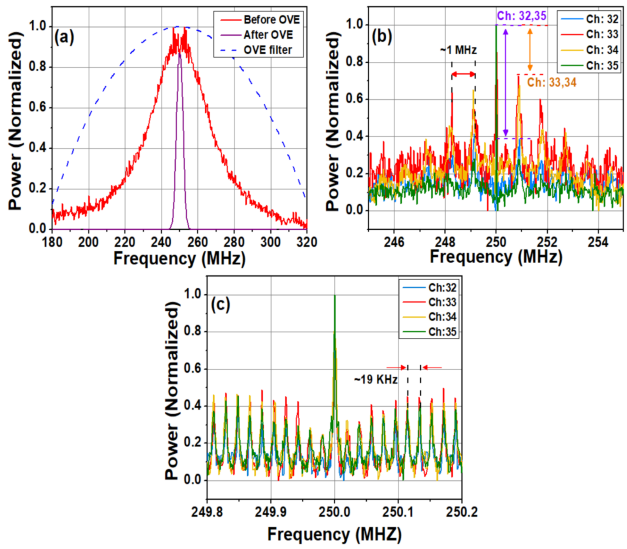

Fig. 6. (a) Linewidth profile obtained by multiplying OVE transmittance curve with experimental data of channel no. 32. Linewidth measurement spectra under OVE for comb line corresponding to WDM channels 32 to 35 with (b) 10 MHz span and (c) 400 kHz span.

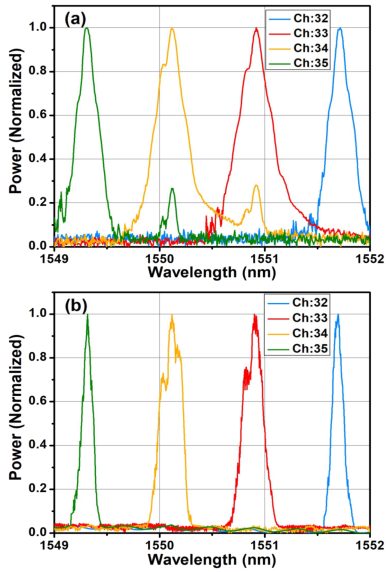

Fig. 7. Optical spectra of the isolated comb lines corresponding to WDM channel no. 32 to 35 observed after OVE at 50% port of C-3 (a) before SOA and (b) after SOA.

effect. As shown in Fig. 5, a large number of fluctuations are still observable near the base of the spectral peak of Fig. 5 (green curves). These variations are the longitudinal modes with FSR of ≈1.03 MHz defined by the FP cavity formed by the 2 × 100 m HNLF modules. The product of the transmittance function of the OVE cavity, described in Section II, with experimentally obtained linewidth data of Ch.32 without OVE is shown in Fig. 6(a). As can be seen from Fig. 6(a) the spectrum narrows down significantly which also indicates narrower linewidth of comb line when OVE is incorporated.

The magnified image of the fluctuations in Fig. 5 with a 10 MHz and 400 KHz span is shown in Fig. 6(b) and (c). From Fig. 6(b) it can be observed that in case of the Ch.33 and Ch.34 (BS-1 and BS-2), the side-modes are separated by ≈1.03 MHz, and are much more distinct than the side-modes of the FWM-generated channels under the Vernier effect. This is because the BS-1 and BS-2 are generated first having Brillouin gain spectra defined by the properties of the 10 km SMF, and in presence of OVE we enforce the cavity to select modes defined by common mode FSR of the composite ring cavity. However, due to the sinusoidal transfer function of a vernier cavity (explained in Section II), the longitudinal modes defined by the FP cavity formed by the HNLF and circulators (FSR ≈1 MHz) that fall under the transfer function curve are also allowed to oscillate. Hence, the signal-to-side-mode power ratio is <15 dB for Ch.33 and Ch.34, with majority of the power lying in the peak wavelengths of BS-1 and BS-2 pumps. Since the power in the peak of the pump wavelengths dominates the FWM process in HNLF, it leads to the generation of FWM-comb lines where the power of the side-modes (1 MHz FSR) is gradually reduced as we move away from the central pump region.

Fig. 6(c) shows the zoomed-in spectrum of Fig. 6(b) by taking the span of 400 kHz. The spectrum shows lines at FSR of 19.6 kHz around the central peak. These lines correspond to the cavity modes due to the 10.4 km fiber inside the unidirectional ring cavity. The FSR of the cavity is 19.6 kHz. The side-modes are >15 dB compared to the central peak, thus giving a >15 dB side-mode suppression. However, it is clear that in our SBS-assisted FWM-based OFC, the FWHM linewidth is reduced from ≈20 MHz as dictated by the Brillouin gain curve, to below 19 KHz by utilizing the optical Vernier effect.

The isolated channels are amplified using SOA of gain 20 dB/channel, which increases the power of the central peak as well as the 1 MHz separated side-modes. The amplified optical and DSH-linewidth spectra before and after SOA are shown in Fig. 7. We have normalized the spectrum in Figs. 7 and 8 for ease of comparison. We observe from Fig. 7(a) and (b), that due to the presence of 1 MHz separated modes in Ch.33 and Ch.34, the OSNR has degraded compared to the FWM-generated lines of Ch.32 and Ch.35 at the SOA output. This is because, the SOA, which is a nonlinear amplifier, amplifies the side-modes and is also responsible for FWM among these modes. This is especially true for pump channels. However, since the power of the side-modes in FWM-generated channels 32 and 35 is less compared to the pumps, amplification and mixing of the side-modes are less in these channels. This can be observed by comparing the linewidth spectra in Fig. 8(a) and (b). As described in section IV-B, this behaviour affects the results of back-to-back PAM transmission. Thus, in the absence of the FC/PC optical connectors inside the cavity, we expect an improved linewidth for each comb line from our OVE setup.

C. B2B OOK and 4-PAM Results

In this section, we discuss the results of the OOK (binary) and 4-PAM B2B transmission experiments using our OFC. The experimental setup is shown in Fig. 9. The amplified isolated OFC lines are modulated by MZM (Covega, Mach-10). The

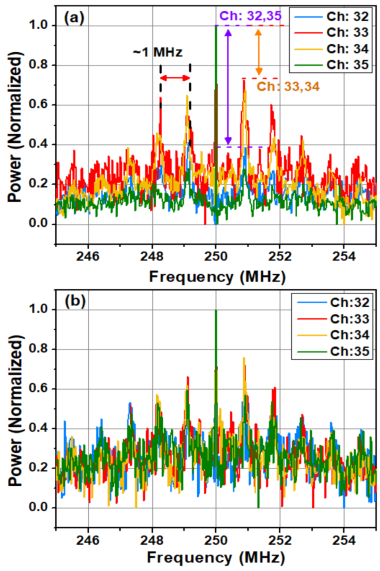

Fig. 8. Linewidth measurement spectra of isolated comb lines corresponding to WDM channel no. 32 to 35 observed after OVE at 50% port of C-3 (a) before SOA and (b) after SOA.

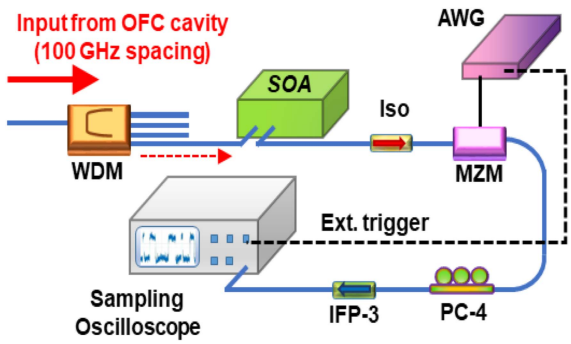

Fig. 9. Setup for pulse amplitude modulation of isolated comb lines. WDM: wavelength division multiplexer, SOA: semiconductor optical amplifier, MZM: Mach-Zehnder modulator, AWG: arbitrary waveform generator, Iso: isolator.

MZM is driven by NRZ-PRBS-2^9 pulses at a data rate of 1 and 10 Gbps using an arbitrary waveform generator (AWG, Keysight M8195 A, $V_{pp} = 1$ V). Figs. 10 and 11(a), (b) show the results of binary-PAM and 4-PAM at 1 Gbps using the eye diagram observed in an 80 GHz sampling oscilloscope (Agilent, DCA-X 86100D) respectively.

From Figs. 10(b), (c), and 11(b) we observe that for channels 33 and 34 (pump channels), the eye diagram shows poor SNR. For the FWM-generated channels as shown in Figs. 10(a), (d), and 11(a) the effect of noise is less compared to the pump channels and the eye is significantly improved. The reason for such degradation in SNR for pump channels is because of the presence of side-modes whose power level increases upon amplification by SOA and hence degrades the SNR. However, the effect of ASE noise in FWM-generated channels (32, 35, and 36) is less compared to the pumps, since the initial power of the side-modes in FWM-generated lines is less. The effect of noise in pump channels is significant in the case of 4-PAM where the eye is almost closed even at a low data rate of 1 Gbps.

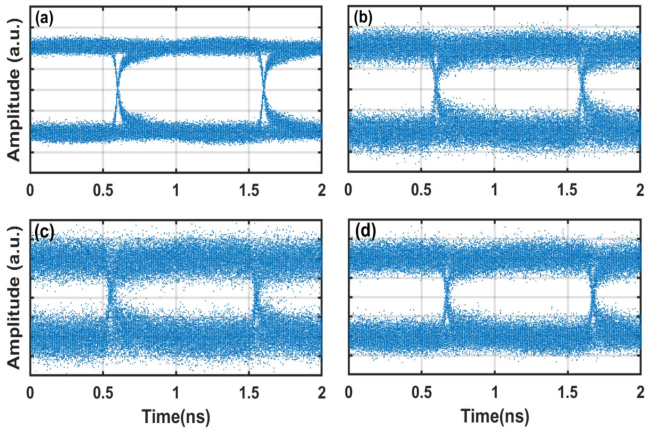

Fig. 10. Eye diagram for binary-PAM with PRBS-2^9-NRZ at 1 Gbps of the isolated comb lines corresponding to WDM channels (a) 32, (b) 33, (c) 34, and (d) 35.

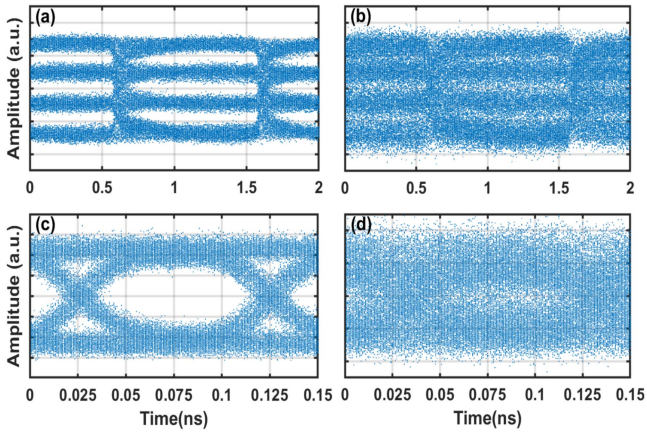

Fig. 11. Eye diagram for 4-PAM at 1 Gbps of the isolated comb lines corresponding to WDM channels (a) 32 and (b) 33. Eye diagram for binary-PAM at 10 Gbps of the isolated comb lines corresponding to WDM channels (c) 32 and (d) 33; with PRBS-2^9-NRZ.

Fig. 11(c) and (d) show the results of 10 Gbps binary-PAM. It is observed from Fig. 11(c) and (d) that the eye of the isolated channels 32 and 33 exhibits a time jitter and poor SNR. This is because of the limited RF drive voltage of V_{pp} of 1 Volt from AWG and the bandwidth limitation of our intensity modulator at 10 GHz.

V. Conclusion

We experimentally demonstrated a low-power, broadband, and narrow linewidth SBS-FWM OFC with tunable line spacing using ≈15 dBm pump power. To the best of our knowledge, this is the lowest pump-power, tunable, and narrow linewidth SBS-FWM OFC having ≈100 nm bandwidth from an all-fiber cavity over the C+L-band to be demonstrated. By tuning the TLSs we are able to achieve variable line spacing from 50 to 600 GHz. We observed that the optical spectra of the SBS-FWM OFC are affected by modulation instability, due to the net anomalous behaviour of the cavity in presence of 10 km SMF. The linewidth of the SBS-assisted FWM comb lines is defined by the SBS pump properties. The OVE is used to significantly

reduce the linewidth of our SBS-FWM OFC by a factor of $\approx 10^3$ compared to OFC without OVE as shown in Fig. 5.

While the OVE reduced the linewidth of generated comb lines to less than 20 kHz, the linewidth of the comb is affected by side-modes due to the FP-cavity formed by the HNLF modules inside the ring configuration in presence of fiber connectors. The presence of side-modes also affects the efficiency of the B2B communication utilizing binary and 4-PAM. We observe that, due to the bandwidth limitation of our electro-optic modulator and the poor flatness of the comb, the data rate was limited to 10 Gbps in B2B transmission for the isolated comb lines. However, with an improved flatness of the OFC and high bandwidth modulators, it is possible to increase the data rate per channel significantly.

REFERENCES

[1] T. Yang, J. Dong, S. Liao, D. Huang, and X. Zhang, "Comparison analysis of optical frequency comb generation with nonlinear effects in highly nonlinear fibers," *Opt. Exp.*, vol. 21, no. 7, pp. 8508–8520, Apr. 2013.

[2] J. L. S. Brito, P. Dainese, and F. C. Cruz, "Optical frequency comb based on single-pass four-wave-mixing in a HNLF combined with EO-modulation," in *Proc. Conf. Lasers Electro- Opt.*, 2016, pp. 1–2.

[3] N. A. Cholan, M. H. Al-Mansoori, A. S. M. Noor, A. Ismail, and M. A. Mahdi, "Self-seeded four-wave mixing cascades with low power consumption," *J. Opt.*, vol. 16, no. 10, Aug. 2014, Art. no. 105203.

[4] M. H. Al-Mansoori and M. A. Mahdi, "Broadly tunable L-band multi-wavelength BEFL utilizing nonlinear amplified loop mirror filter," *Opt. Exp.*, vol. 19, no. 24, pp. 23981–23988, Nov. 2011.

[5] K. Zhu, J. He, K. Chang, D. Xing, Y. Liu, and Z. Wang, "Tunable and narrow linewidth multi-wavelength Brillouin-Erbium fiber laser using dual-wavelength pumping," *Optoelectron. Lett.*, vol. 18, no. 6, pp. 349–353, Jun. 2022.

[6] P. Wang et al., "Multi-wavelength fiber laser generated by Brillouin-comb assisted four-wave mixing," *Opt. Commun.*, vol. 444, pp. 63–67, 2019.

[7] N. A. B. Ahmad, S. H. Dahlan, and N. A. Cholan, "Four-wave mixing cascades seeded by a multiwavelength Brillouin–Erbium fiber laser," *Laser Phys.*, vol. 28, no. 9, Jul. 2018, Art. no. 095102.

[8] E. Pedruzzi, L. C. Silva, A. G. Leal-Junior, and C. E. Castellani, "Generation of a multi-wavelength Brillouin Erbium fiber laser with low threshold in multiple frequency spacing configurations," *Opt. Fiber Technol.*, vol. 69, 2022, Art. no. 102832.

[9] A. Al-alimi, M. Yaacob, A. Abas, M. Mahdi, M. Al-Mansoori, and M. Mokhtar, "Simple multiwavelength Brillouin–Erbium-doped fiber laser structure based on short SSMF," *Opt. Commun.*, vol. 300, pp. 8–11, 2013.

[10] H. Zou, R. Yang, X. Shen, and W. Wei, "Stable and tunable self-seeded multiwavelength Brillouin-Erbium fiber laser with higher OSNR," *Opt. Laser Technol.*, vol. 81, pp. 180–183, 2016.

[11] L. Ma, H. Zou, H. Xiong, H. Wu, and Y. Zhang, "Multiwavelength generation by using a novel Brillouin-Erbium fiber laser with double linear-cavity based on a double-pass Brillouin Pump (BP) amplification technique," *Opt. Laser Technol.*, vol. 117, pp. 169–174, 2019.

[12] X. Ge, F. Zhang, and S. L. Pan, "Stimulated Brillouin scattering based optical frequency comb generation using a stocks wave recycling loop," in *Proc. IEEE 13th Int. Conf. Opt. Commun. Netw.*, 2014, pp. 1–3.

[13] I. Golub, A. Atieh, and P. Mohanan, "Comparison of different schemes for stimulated Brillouin scattering enhancement," *Appl. Opt.*, vol. 58, no. 3, pp. 545–548, Jan. 2019.

[14] G. P. Agrawal, *Nonlinear Fiber Optics*. Cambridge, MA, USA: Academic Press, 2012.

[15] M. Ferreira, J. Rocha, and J. Pinto, "Analysis of the gain and noise characteristics of fibre Brillouin amplifiers," *Springer Opt Quant Electron*, vol. 26, pp. 35–44, 1994.

[16] I. Victor L. et al., "Temporal characterization of a multi-wavelength Brillouin–Erbium fiber laser," *New J. Phys.*, vol. 18, no. 8, May 2016, Art. no. 055003.

[17] W. Peng et al., "A tunable self-seeded Brillouin/Erbium fiber laser utilizing an asymmetrical twin-core fiber-based Mach–Zehnder interferometer," *Laser Phys.*, vol. 23, no. 3, 2013, Art. no. 035101.

[18] L. Qian, D. Fen, H. Xie, and J. Sun, "A novel tunable multi-wavelength Brillouin fiber laser with switchable frequency spacing," *Opt. Commun.*, vol. 340, pp. 74–79, 2015.

[19] H. Xie, J. Sun, D. Feng, and L. Qian, "Compact multiwavelength Brillouin fiber laser by utilizing EDF as hybrid gain media," *IEEE Photon. J.*, vol. 7, no. 6, Dec. 2015, Art. no. 1504110.

[20] A. Paul and P. K. Krishnamurthy, "All-SBS fiber-based setup for optical frequency comb generation utilizing a pump recycling technique and comb line isolation by implementing Brillouin amplification," *Appl. Opt.*, vol. 61, no. 29, pp. 8799–8805, Oct. 2022.

[21] G. Gan, K. Yeo, F. M. Adikan, and Y. Shee, "Four-wave-mixing-assisted Brillouin fiber laser with double-Brillouin-frequency spacing," *Opt. Fiber Technol.*, vol. 21, pp. 198–201, 2015.

[22] Z. Wang, T. Wang, Q. Jia, W. Ma, Q. Su, and P. Zhang, "Triple Brillouin frequency spacing multiwavelength fiber laser with double Brillouin cavities and its application in microwave signal generation," *Appl. Opt.*, vol. 56, no. 26, pp. 7419–7426, Sep. 2017.

[23] M. K. Awsaj et al., "Tunable 60 GHz multiwavelength Brillouin Erbium fiber laser," *Appl. Sci.*, vol. 13, no. 5, 2023, Art. no. 3275.

[24] Z. Zhou, Q. Yang, Y. Chen, M. Chen, and Z. Zhang, "Tunable Brillouin-Raman multi-wavelength fiber laser with a linear cavity configuration," *Physica Scripta*, vol. 97, no. 9, Aug. 2022, Art. no. 095502.

[25] J. Tang, J. Sun, L. Zhao, T. Chen, T. Huang, and Y. Zhou, "Tunable multiwavelength generation based on Brillouin-Erbium comb fiber laser assisted by multiple four-wave mixing processes," *Opt. Exp.*, vol. 19, no. 15, pp. 14682–14689, Jul. 2011.

[26] N. Cholan, M. Al-Mansoori, A. Noor, A. Ismail, and M. Mahdi, "Formation, properties and role of residual waves as seeds in multiwavelength Brillouin-Erbium fiber laser," *Opt. Commun.*, vol. 329, pp. 163–167, 2014.

[27] W. Gao et al., "Multi-wavelength Brillouin-Erbium fiber laser with more than 95 lines based on a dual-ring structure," *Japanese J. Appl. Phys.*, vol. 58, no. 8, Jul. 2019, Art. no. 082003.

[28] L. Qing et al., "Optical frequency combs generated by four-wave mixing in a dual wavelength Brillouin laser cavity," *AIP Adv.*, vol. 7, Feb. 2017, Art. no. 075215.

[29] F. Wang, M. Peng, L. Shi, W. Kang, and J. Huang, "A stable multi-wavelength fiber linear cavity laser based on cascaded four-wave mixing in highly nonlinear fiber," in *Proc. Int. Photon. Optoelectron. Meeting*, 2018, Art. no. OT4A.62.

[30] Y. Shi et al., "Wideband multiwavelength Brillouin fiber laser with switchable channel spacing," *Appl. Opt.*, vol. 62, no. 8, pp. 2130–2136, Mar. 2023.

[31] Y. Pang, Y. Xu, X. Zhao, Z. Qin, and Z. Liu, "Stabilized narrow-linewidth Brillouin random fiber laser with a double-coupler fiber ring resonator," *J. Lightw. Technol.*, vol. 40, no. 9, pp. 2988–2995, May 2022.

[32] O. Pottiez et al., "Supermode noise of harmonically mode-locked erbium fiber lasers with composite cavity," *IEEE J. Quantum Electron.*, vol. 38, no. 3, pp. 252–259, Mar. 2002.

[33] Y. Pang et al., "Frequency comb generation based on Brillouin random lasing oscillation and four-wave mixing assisted with nonlinear optical loop mirror," *Photonics*, vol. 10, no. 3, Mar. 2023, Art. no. 296.

[34] R. W. Boyd, *Nonlinear Optics*. New York, NY, USA: Elsevier Science, 2008.

[35] O. A. Nieves, M. D. Arnold, M. J. Steel, M. K. Schmidt, and C. G. Poulton, "Numerical simulation of noise in pulsed Brillouin scattering," *J. Opt. Soc. Amer. B*, vol. 38, no. 8, pp. 2343–2352, Aug. 2021.